Cell Death & Differentiation (2021) 28:2571–2588
https://doi.org/10.1038/s41418-021-00772-5

Cell Death & Differentiation

ARTICLE

Hevin–calcyon interaction promotes synaptic reorganization after brain injury

Jong-Heon Kim[1] · Hyun-Gug Jung[2,3] · Ajung Kim[2] · Hyun Soo Shim[4] · Seung Jae Hyeon[4] · Young-Sun Lee[3] · Jin Han[5] · Jong Hoon Jung[6] · Jaekwang Lee[6] · Hoon Ryu[4,7,8] · Jae-Yong Park[3] · Eun Mi Hwang[2] · Kyoungho Suk[1,5]

Received: 15 July 2020 / Revised: 2 March 2021 / Accepted: 4 March 2021 / Published online: 22 March 2021
© The Author(s), under exclusive licence to ADMC Associazione Differenziamento e Morte Cellulare 2021

Abstract

Hevin, also known as SPARC-like protein 1 (SPARCL1 or SC1), is a synaptogenic protein secreted by astrocytes and modulates the formation of glutamatergic synapses in the developing brain by interacting with synaptic adhesion proteins, such as neurexin and neuroligin. Here, we identified the neuron-specific vesicular protein calcyon as a novel interaction partner of hevin and demonstrated that this interaction played a pivotal role in synaptic reorganization after an injury in the mature brain. Astrocytic hevin was upregulated post-injury in a photothrombotic stroke model. Hevin was fragmented by MMP3 induced during the acute stage of brain injury, and this process was associated with severe gliosis. At the late stage, the functional hevin level was restored as MMP3 expression decreased. The C-terminus of hevin interacted with the N-terminus of calcyon. By using RNAi and binding competitor peptides in an ischemic brain injury model, we showed that this interaction was crucial in synaptic and functional recoveries in the sensory-motor cortex, based on histological and electrophysiological analyses. Regulated expression of hevin and calcyon and interaction between them were confirmed in a mouse model of traumatic brain injury and patients with chronic traumatic encephalopathy. Our study provides direct evidence for the causal relationship between the hevin–calcyon interaction and synaptic reorganization after brain injury. This neuron-glia interaction can be exploited to modulate synaptic reorganization under various neurological conditions.

Introduction

Recovery after brain injury is a multi-step process that encompasses tissue remodeling, synaptic reorganization, and functional plasticity. The synaptic reorganization is a form of brain plasticity and includes a formation of new sprouted circuits composed of excitatory and inhibitory neurons. Although synaptic organization relies on the connection between neuronal cells, over the past decades,

These authors contributed equally: Jong-Heon Kim, Hyun-Gug Jung

Edited by P. Salomoni

Supplementary information The online version contains supplementary material available at https://doi.org/10.1038/s41418-021-00772-5.

✉ Eun Mi Hwang
emhwang@kist.re.kr

✉ Kyoungho Suk
ksuk@knu.ac.kr

[1] Brain Science & Engineering Institute, Kyungpook National University, Daegu, Republic of Korea

[2] Center for Functional Connectomics, Brain Science Institute, Korea Institute of Science and Technology, Seoul, Korea

[3] School of Biosystems and Biomedical Sciences, College of Health Science, Korea University, Seoul, Republic of Korea

[4] Center for Neuroscience, Brain Science Institute, Korea Institute of Science and Technology, Seoul, Korea

[5] Department of Pharmacology and Department of Biomedical Science, School of Medicine, Kyungpook National University, Daegu, Republic of Korea

[6] Research Group of Functional Food Materials, Korea Food Research Institute, Wanju, Republic of Korea

[7] VA Boston Healthcare System, Boston, MA, USA

[8] Boston University Alzheimer's Disease Center and Department of Neurology, Boston University School of Medicine, Boston, MA, USA

astrocytes have been identified as a third key component of the synaptic machinery [1] and their crucial roles in structural synaptic formation [2–4] have been demonstrated. Astrocytes release various non-structural matricellular proteins containing an extracellular matrix (ECM)-interacting domain during CNS development. These proteins not only serve as stable structural elements in the extracellular space but also play regulatory roles, such as tissue remodeling [5]. Expression of astrocytic matricellular proteins is mostly induced during CNS development and repressed in the mature brain [5]; however, hevin expression has been shown to be sustained in the mature brain [6].

Reactive astrocytes around the central lesion core form a densely intertwined glial scar. Meanwhile, some of the reactive astrocytes in the peri-lesion area actively interact with viable neurons and perform diverse functions associated with amelioration of CNS afflictions, tissue repair, or synaptic reorganization [7]. Reactive astrocytes in this area release matricellular proteins to the damaged tissue [5, 8–10], implying a crucial role of matricellular proteins in tissue repair [11–13] or synaptic reorganization [9, 14] after CNS injury. However, the precise role of astrocytic matricellular proteins under pathological conditions is not fully uncovered.

Hevin, one of the matricellular proteins, has recently been identified as a novel synapse organizer during normal brain development [3, 15]. During CNS development, astrocytic hevin acts as a bridge interacting with presynaptic neurexin-1α and postsynaptic neuroligin-1 (NLG1) to form the initial synaptic structure by recruiting N-methyl-D-aspartate receptor (NMDAR) in glutamatergic synapses [15]. Hevin has been reported to undergo proteolytic post-translational modification. Interestingly, protein sequencing of hevin digested by MMP3, a primarily inducible protease in the inflamed brain [16], revealed that the major proteolytic product was similar to "secreted protein acidic and rich in cysteine" (SPARC) in primary structure and function [17]. SPARC and "SPARC-like fragment from a full length of hevin" (SLF) may have antagonistic activity against hevin [3]. These previous studies suggest that the synaptogenic role of hevin may be regulated by protease activity under pathological conditions. However, the precise molecular mechanisms underlying protease-mediated regulation of hevin are not fully understood. In the present study, we explored the role of hevin during synaptic recovery in the adult brain.

Materials and methods

Photothrombotic stroke (PTS)

Adult C57BL/6 male mice (7–8-week-old) were anesthetized by isoflurane. Rose Bengal was intraperitoneally injected with a dose of 100 mg per body weight (kg). After 10 min, a green light laser (540 nm, 20 mW) giving an illumination with 2-mm diameter was positioned on the sensorimotor cortex (1.5 mm right from Bregma) through the intact skull for 20 min.

Immunohistochemistry

Mice were euthanized by inhalation of an overdose of ether. They were then subjected to intracardiac perfusion-fixation using 0.9% NaCl and 4% paraformaldehyde (PFA) dissolved in 0.1 M PBS (pH 7.4). Isolated brains were immersion-fixed in 4% PFA for 72 h. For cryoprotection, the brains were incubated for 72 h in 30% sucrose diluted in 0.1 M PBS, embedded in optimal cutting temperature (OCT) compound (Tissue-Tek; Sakura Finetek, Torrance, CA), and cut into 12-μm-thick coronal or sagittal sections. Hevin and SPARC immunostaining were performed as previously described but with slight modifications [3]. Briefly, the sections were dried at 37 °C for 30 min and three times rinsed with 0.1 M PBS solution to remove the OCT compound and blocked using 50% normal donkey serum with 0.5% Triton X-100 in PBS solution for 1 h at room temperature. Brain sections were incubated with goat anti-hevin polyclonal primary antibody (1:500; R&D Systems, AF2836), rabbit anti-glial fibrillary acidic protein (GFAP) antibody (1:1000; DakoCytomation, N1506), rat anti-complement component 3 (C3) antibody (1:200; Novus Biologicals, NB200-540), or mouse anti-S100A10 antibody (1:200; Thermo, MA5-24769) overnight at 4 °C. After three times rinsing with PBS, the sections were incubated for 2 h at room temperature with the following secondary antibodies: FITC-conjugated donkey anti-rabbit IgG antibodies (1:200; 711-096-152), Cy3-conjugated donkey anti-goat IgG antibodies (1:200; 705-165-147), Cy5-conjugated donkey anti-mouse IgG antibodies (1:200; 715-175-151) (Jackson ImmunoResearch Laboratories, West Grove, PA). The sections were then mounted and counterstained using gelatin-containing 4′,6-diamidino-2-phenylindole (DAPI, Vector Laboratories). Tiled images of each section were captured using a CCD color video camera (Ximena, Münster, Germany) through an objective lens attached to a microscope (Leica Microsystems, Wetzlar, Germany). Photomicrographs were obtained, and the number of hevin-positive astrocytes was counted in the unit area (mm^2). For the assessment of synaptic puncta in vivo [3, 18], a blocking solution containing 20% normal donkey serum in PBS (without Triton X-100) was used. The blocked sections were incubated with antibodies against presynaptic marker [rabbit anti-VGLUT-2 (1:2000; Synaptic Systems, 135 404) and postsynaptic marker [mouse anti-PSD-95 (1:500; 6G6-1C9 clone; Thermo, MA1-045)] in PBS with 0.3% Triton X-100 and 10% NDS for 60 h at 4 °C, and then with FITC-conjugated donkey anti-rabbit IgG antibodies (1:200; 711-

096-152) and Cy5-conjugated donkey anti-mouse IgG antibodies (1:200; 715-175-151) (Jackson ImmunoResearch Laboratories, West Grove, PA). Merged images (150 × 150 μm) of the sensorimotor cortex were obtained by using a laser scanning confocal microscope. A z-stack for each section was collected for a total depth of 5 μm (15 × 0.33 μm optical sections). Maximum image projections (MIPs) were generated for groups of three consecutive optical sections yielding five MIPs/section each representing 1 μm of depth. Colocalized puncta were measured with a custom plug-in for the NIH image-processing package ImageJ [18].

Plasmids

cDNAs encoding for full-length mouse hevin (GenBank accession no. NM_010097) and mouse calcyon (NM_026769) were obtained by using an RT–PCR-based Gateway cloning method (Invitrogen). Mutant forms of hevin and calcyon were also generated using full-length cDNAs as templates via the EZchange site-directed mutagenesis kit (Enzynomics). The target region of shRNA is as follows: mouse calcyon: 5′-ggacacgagagagaaagaaga-3′; mouse hevin: 5′-gcagctttatgaaccaaatcc-3′. Calcyon shRNA-insensitive form (5′-agataccagggaaaaggagga-3′) was obtained by performing oligonucleotide-directed mutagenesis using the EZchange site-directed mutagenesis kit. The constructs were cloned into several vectors, including pDEST-GFP-N, pDEST-HA-C, and pDEST-HA-N by gateway cloning.

Virus production

The validated mouse shRNA sequence for hevin, calcyon, or shRNA-insensitive form of calcyon cDNA were cloned into the pSicoR vector (Addgene, Cambridge, MA) and subcloned into the pAAV-MCS vector (Stratagene, San Diego, CA). Using these viral vectors, AAV was packaged at KIST Virus Facility (http://virus.kist.re.kr).

Yeast two hybrid (Y2H) screening and assay

Calcyon–N was ligated into the GAL4 DNA binding domain (BD), and Hevin–N and -C regions were cloned into the activation domain (AD). To assess the protein-protein interaction between Calcyon-N and Hevin-C, the yeast strain AH109 was co-transformed with BD/Caclyon-N and AD/Hevin-C and incubated in the selection medium.

Bimolecular fluorescence complementation (BiFC) assay

Calcyon and hevin were cloned into the bimolecular fluorescence complement vectors pBiFC-VN173 and pBiFC-VC155. To confirm the expression of each BiFC vector, additional Flag and HA tags were inserted in the C-terminal region of both BiFC vectors. HEK293T cells were co-transfected with the cloned BiFC vectors in all possible pairwise combinations. The next day, these cells were fixed with 4% paraformaldehyde for 20 min at room temperature and permeabilized with 0.3% Triton X-100 for 5 min. After blocking for 1 h, the cells were incubated with rat anti-HA (1: 500, 3F10, Roche Applied Science) and mouse anti-Flag (1:500, M-2, Sigma-Aldrich, F3165) antibodies at 4 °C overnight. Then, the cells were incubated with Alexa Fluor 594- or 647-conjugated secondary antibodies (Jackson ImmunoResearch Laboratories) for 1 h and then stained with DAPI to visualize nuclei. All images were acquired by confocal microscopy on a Nikon A1 confocal microscope.

Cell culture

HEK293T cells were purchased from the Korean Cell Line Bank (Seoul National University, Seoul, Korea) and cultured in DMEM (Invitrogen) containing 10% fetal bovine serum (Invitrogen) and 100 units/ml penicillin-streptomycin at 37 °C in a humidified atmosphere of 95% air and 5% CO_2. Neonatal astrocyte cultures were prepared from mixed glial cultures as described previously, with minor modifications [19]. In brief, whole brains of 3-day-old C57BL/6 mice were chopped and mechanically disrupted using a nylon mesh. The cells obtained were seeded in culture flasks and grown in DMEM containing 10% FBS, 100 U/ml penicillin, and 100 μg/ml streptomycin at 37 °C in a humidified atmosphere of 95% air and 5% CO_2. Culture media were changed initially after 7 days and then every 3 days. Cells were used after culture for 14 days in vitro (DIV). Primary astrocytes were obtained by shaking mixed glial cultures at 250 rpm overnight. Culture media including other cell types were aspirated, and astrocytes were dissociated using trypsin-EDTA (Invitrogen) and collected by centrifugation at 5000 × *g* for 10 min. Primary astrocytes were grown and maintained in DMEM supplemented with 10% FBS and penicillin-streptomycin. Primary cultures of cerebral cortical neurons were prepared from embryonic day 18 mice as described previously [20]. Briefly, mouse embryos were decapitated and the brains were rapidly placed in a culture dish containing cold PBS. Cortices were isolated, transferred to a culture dish containing 0.25% trypsin-EDTA in PBS, incubated for 30 min at 37 °C, and then washed twice in serum-free neurobasal medium (Invitrogen). The cortical tissue was mechanically dissociated by gentle pipetting, and the resulting dissociated cortical cells were seeded onto plates or cover glasses coated with poly-D-lysine (Sigma-Aldrich). The cells were then cultured in the neurobasal medium containing 2 mM glutamine (Sigma-Aldrich), penicillin-streptomycin, nerve

growth factor (Invitrogen), N2 supplement (Invitrogen), and B27 supplement (Invitrogen).

Concentration of secreted proteins

HEK293T cells were transfected with several plasmids (Hevin-ΔSP-Flag, Hevin-Flag, Hevin-Δ31aa-Flag, and SPARC-Flag). After 24 h, the medium was replaced with DMEM, and the cells were incubated for an additional 24 h. Then, supernatants were collected for further analysis. Secreted proteins were concentrated as previously described with minor modifications [21]. Briefly, debris and dead cells were removed by centrifuging the sample at 2000 × *g* for 10 min at 4 °C. Protease inhibitor cocktail was added to the samples. Secreted proteins in culture media were concentrated through ultrafiltration using Amicon Ultra-15 centrifugal filter unit (Millipore) according to the manufacturer's instructions. The total amounts of proteins were determined using a BCA assay (Thermo Fisher).

Coimmunoprecipitation (Co-IP) and immunoblotting assays

Whole-cell lysates were mixed overnight at 4 °C with 3 μg of mouse anti-GFP (B-2; Santa Cruz Biotechnology, sc-9996) or rabbit anti-calcyon (Cloud-Clone Corp., Houston, TX, USA, PAD980Mu01) antibody in the lysis buffer (50 mM Tris–HCl, pH 7.4; 150 mM NaCl; 5 mM EDTA; 1 mM PMSF; and 1% NP-40) containing a protease inhibitor cocktail (Roche). Immune complexes were incubated with protein A/G PLUSAgarose (Santa Cruz Biotechnology) for 1 h and then washed four times with the lysis buffer. For brain tissue co-IP, tissues were dissected from the peri-injury region and stored at −80 °C. The frozen brains were washed with 5 ml of cold modified Dulbecco's phosphate-buffered saline (DPBS, Gibco) and homogenized in ice-cold lysis buffer (10 μl/μg) containing 25 mM Tris-HCl (pH 7.4), 150 mM NaCl, 1 mM EDTA, 1% Nonidet P-40, 5% glycerol, protease inhibitors (Roche Applied Science, Basel, Switzerland), and phosphatase inhibitors (Roche Applied Science) using a tissue grinder and passed through a syringe ten times. The homogenate was centrifuged for 30 min at 14,000 × *g* and 4 °C. The supernatant was transferred to a new tube, and the pellet containing cell debris was discarded. For the pre-cleaning of the lysate, the supernatant was mixed with pre-washed G-Sepharose beads (Protein G, GE Healthcare) and incubated on a rocking platform for 1 h at 4 °C. After centrifugation at 1000 × *g* for 10 min, the supernatant was transferred to a new tube, and 50 μl of it was saved as the input control. The lysate was incubated with an appropriate amount (0.1 μg/μg protein) of non-immune sera or antibodies [goat anti-hevin (R&D Systems, AF2836), rabbit anti-calcyon (Cloud-Clone Corp., Houston, TX, USA, PAD980Mu01), mouse anti-GFP (B-2, Santa Cruz Biotechnology, sc-9996), rabbit anti-mCherry (Invitrogen, PA5-34974), and mouse anti-Flag (M-2, Sigma-Aldrich, F3165)] overnight at 4 °C. Then, pre-washed beads (100 μl/μg protein) were mixed with the lysate in DPBS on a rocking platform overnight at 4 °C. Following three washes with ice-cold DPBS, the lysate-bead mixture was centrifuged at 3000 × *g* for 3 min. For secreted protein coimmunoprecipitation, 250 μg of concentrated secreted proteins (Hevin-ΔSP-Flag, Hevin-Flag, Hevin-Δ31aa-Flag, and SPARC-Flag) were mixed with HA-Calcyon-transfected HEK293T cell lysates for 1 h at 4 °C. Five percent of the mixture was saved as the input control. The lysate mixture was incubated with mouse anti-Flag (M-2, Sigma-Aldrich, F3165) antibody (3 μg) and protein A/G PLUS Agarose (Santa Cruz Biotechnology) for 30 min. The mixture complex was placed on rotator for overnight at 4 °C. After washing three times with ice-cold DPBS containing protease inhibitor cocktail, the lysate-bead complex was centrifuged at 2000 rpm. For immunoblotting, protein samples were resolved by 10% or 15% SDS–PAGE. The resolved proteins were transferred onto polyvinylidene fluoride membranes. The blots were incubated overnight at 4 °C with the rat anti-HA (1:1000, 3F10; Roche Applied Science), mouse anti-GFP (1:1000, B-2; Santa Cruz Biotechnology, sc-9996), rabbit anti-mCherry (Invitrogen, PA5-34974), goat anti-hevin (1:1000; R&D Systems, AF2836), goat anti-SPARC (1:1000; R&D Systems, AF942), rabbit anti-GFAP (1:1000; DakoCytomation, Glostrup, Denmark, N1506), rabbit anti-S100b (1:1000; DakoCytomation, Glostrup, Denmark, GA504), mouse anti-PSD-95 (1:1000, 6G6-1C9 clone; Thermo, MA1-045), rabbit anti-VGLUT-2 (1:1000; Synaptic Systems, 135 404), rabbit anti-calcyon (1:500; Cloud-Clone Corp., PAD980Mu01), rabbit anti-NLG1B (1:1000; Synaptic systems, 129 013), anti-β-actin (1:5000; Thermo Scientific, MA5-15739), or anti-α tubulin (1:5000; Sigma-Aldrich, T8203) antibodies. Blots were then washed and incubated with horseradish peroxidase-conjugated anti-rabbit, anti-rat, or anti-mouse IgG antibodies. After a final wash, the immunoreactivity of the blots was evaluated with enhanced chemiluminescence (Amersham Biosciences).

Duolink-proximity ligation assay (PLA) in neurons

PLA assay was performed in mouse primary cortical neurons to determine whether secreted Hevin physically interacts with Calcyon. Before PLA assay, neuron cultures (DIV8) were transiently transfected with PSD95-mCherry construct using Neuromag (OZ Biosciences). PLA assay was conducted according to the manufacturer's instructions (Sigma-Aldrich). Briefly, cells were incubated with several proteins (Hevin-ΔSP-Flag, Hevin-Flag, Hevin-Δ31aa-Flag,

and SPARC-Flag) for 1 h at 4 °C. Following incubation, cells were washed with PBS, fixed in 4% PFA for 15 min. After incubation with a blocking buffer for 1 h, the cells were incubated with the primary antibodies against Flag (1:200, M-2, Sigma-Aldrich, F3165) and Calcyon (1:200, Cloud-Clone Corp., PAD980Mu01). Donkey anti-rabbit PLAplus and donkey anti-mouse PLAminus probes were applied, followed by ligation and amplification with Duolink detection reagent Green according to the manufacturer's instructions. Neuronal structure was visualized by addition of chicken anti-MAP2 antibody (1:2000, Abcam, ab5392) and Alexa Fluor 647 (Jackson Immunoresearch, 115-605-003).

Immunocytochemical analysis of HEK293T

HEK293T cells seeded on coverslips were transfected with HA-Calcyon-GFP or Calcyon-HA-GFP for 24 h, and fixed with 4% PFA. HA-tag staining was conducted under two different conditions; non-permeabilizing and permeabilizing conditions. Cells were permeabilized by treating with 0.3% Triton X-100 for 7 min. Non-permeabilized cells were maintained with DPBS. Then, two groups of cells were subjected to the same staining protocol. The coverslips were blocked in 3% BSA/5% normal donkey serum and incubated with a rat anti-HA antibody (1:500, 3F10, Roche Applied Science) for overnight at 4 °C. On the next day, the cells were incubated with Alexa 594-conjugated secondary antibody (Jackson Immunoresearch, 111-585-003) for 1 h and then stained with DAPI. All images were acquired by confocal microscopy (Nikon A1).

Immunocytochemical analysis and synapse quantification on cortical or cortical/thalamic neurons

Immunocytochemical analysis of synapses was performed as previously described, with minimal modifications [18]. Neurons were cultured for 3 days, and were treated with AraC. Afterward, neuron cultures were treated with hevin (90 nM) or vehicle twice at DIV 8 and DIV 11. Cortical or cortical/thalamic neurons were incubated for 10 min at room temperature with 4% paraformaldehyde (PFA) prewarmed to 37 °C to fix synaptic proteins and then rinsed three times with PBS solution. Subsequently, the samples were blocked with a blocking buffer containing 50% normal donkey serum (NDS) and 0.2% Triton X-100 for 30 min. Then, they were rinsed three times with PBS solution, and the primary antibodies diluted in the 10% NDS-containing antibody diluent solution were added to each well. These antibodies recognized a presynaptic marker [rabbit anti-synaptotagmin 1/2 (1:1000, cytosolic domain; Synaptic Systems, 105 003)], excitatory presynaptic marker [VGlut1 (1:1000; Sigma-Aldrich, AB5905), VGlut2 (1:1000; Synaptic Systems, 135 404)], and postsynaptic marker [mouse anti-PSD95 (1:500, 6G6-1C9 clone; Thermo, MA1-045)]. The samples were incubated for 48 h at 4 °C, rinsed three times with PBS, and incubated with the following secondary antibodies: FITC-conjugated donkey IgG (1:200) or Cy5-conjugated donkey IgG (1:200) (Jackson ImmunoResearch Laboratories, West Grove, PA). After incubating for 2 h at room temperature, the samples were rinsed three times with PBS and mounted in Vectashield mounting medium with DAPI on glass slides. Merged images were assessed for colocalized puncta with a custom plug-in, Puncta analyzer, for the NIH image-processing package ImageJ or Neurolucida 360 (version 2020.3.2., MBF Biosciences, Williston, VT).

Viral infection and intracortical injection

For inducible knockdown of calcyon and hevin, burr holes were made with drilling into the skull, and viral administration was unilaterally performed with a gentle drip of 3 µl vector per brain injury region under sterile conditions. Intracortical administration was performed using a brain infusion kit and osmotic pump injections. Following the brain injury, a brain infusion cannula (Brain Infusion Kit 3; ALZET, Cupertino, CA, USA) and Alzet osmotic pump (1002, 0.5 mL/h; ALZET, Cupertino, CA) were implanted into the infarct region and cemented with super-glue.

Neurological functional recovery test

For the adhesive removal test (tape test), a small adhesive patch (rectangular 0.35×0.45 cm^2) was applied to the forelimb contralateral to the photothrombotic hemisphere. The mouse was then put into a cage and the time to make contact and remove the adhesive tape was recorded with 120 s being the time limit. To remove the tape, mouse would raise both forelimbs toward their face and swipe off the tape with both forepaws. To assess motor coordination and balance alterations in the mice, an accelerated RotaRod test was performed. RotaRod apparatus (Panlab, Harvard Apparatus) consisted of a striated rod providing a nylon cylinder (diameter: 3 cm) separated into four regions (width: 5 cm) and located 20 cm above the floor grid. One day before the brain injury, mice were placed on the rod for 30 s without rotation, followed by 120 s of low-speed rotation at 4 rpm. Subsequently, the mice were tested in three trials for 5 min each (4–40 rpm). After the brain injury, the mice were tested under the same conditions at the indicated time periods. During each trial, the latency to fall was recorded.

Brain slice preparation

Cortical slices (thickness 300 µm) were obtained from virus-infected C57BL/6 mice at 21-dpi after cortical injury. Following decapitation, the brain was rapidly removed and placed in cold artificial cerebrospinal fluid (ACSF) having the following composition (in mM): 130 NaCl, 3.5 KCl, 0.5 $CaCl_2$, 24 $NaHCO_3$, 3 $MgCl_2$, 1.25 NaH_2PO_4, and 10 glucose. The slices were made using an oscillating tissue slicer (Leica VT1000s) at 4 °C and stored in a bath of oxygenated (95% O_2, 5% CO_2) ACSF for a recovery period of at least 1 h at room temperature. Each slice that was studied was transferred from a recovery/holding reservoir to the recording chamber of a fixed-stage upright microscope (Olympus BX51WI) and submerged in oxygenated ACSF that was supplied to the chamber at a rate of 1.5–2 ml/min. The composition of the ACSF used to perfuse the recording chamber was changed to 1.5 $CaCl_2$ and 1.5 $MgCl_2$. The submerged slice was visualized either directly via the microscope's optics, or indirectly via a high-resolution CCD camera system (optiMOS, Qimaging) that received the output of a CCD camera attached to the microscope's video port.

Electrophysiology

Whole-cell patch-clamp recordings were obtained using borosilicate glass pipettes (resistance 4–6 MΩ) prepared using a 2-stage vertical pipette puller (P-1000, Shutter instrument). The pipettes were filled with a solution having the following composition (in mM): 130.0 CsCl, 2.0 $MgCl_2$, 2.0 $CaCl_2$, 2.0 Na-ATP, 0.2 Na-GTP, 10 HEPES, 0.5 EGTA, 10.0 Glucose; pH was adjusted to 7.2 with CsOH. Patch recordings were obtained from cortical neurons and used to obtain spontaneous EPSC. Voltage-clamp and current-clamp recordings were acquired using a Multi-Clamp 700B amplifier, using pClamp10 software (Molecular Devices, Union City, CA, USA). All patch recordings were from layer 2–3 pyramidal neurons located near the scar of damaged region (about 100 µm from brain scar). Sampling rate of all recordings was 5 kHz. No correction for liquid junction potential was made.

Reverse transcription-PCR and RNA-seq

Total RNA was extracted from cells or tissues using the TRIzol reagent (Life Technologies) according to the manufacturer's instructions. Reverse transcription was performed using Superscript II (Invitrogen) and oligo (dT) primers. Traditional PCR amplification using the specific primer sets [*mmp3*: forward (5′-CTGTGTGTGGTTGTGT GCTCATCCTAC-3′) and reverse (5′-GGCAAATCCGGT GTATAATTCACAATC-3′), a*damts4*: forward (5′-CAT CCGAAACCCTGTCAACTTG-3′) and reverse (5′-GCCC ATCATCTTCCACAATAGC-3′), g*apdh*: forward (5′-CGC CCTTGAGCTAGGACTG-3′ and reverse (5′-CTCGCT CCTGGAAGATGGTG-3′)] was performed at an annealing temperature of 55–60 °C with 25–30 cycles in a C1000 Touch Thermal Cycler (Bio-Rad). To analyze the PCR products, 10 µl of each PCR sample was electrophoresed on an agarose gel, which was then stained with ethidium bromide and observed under ultraviolet light. To determine human *MMP3* mRNA levels, the RNA sequencing data [European Nucleotide Archive (ENA) database under accession no. ERP015139] from normal postmortem brains and those with chronic traumatic encephalopathy (CTE) were analyzed [22]. The relative *MMP3* mRNA levels were calculated as fold changes of FPKMs (Fragments Per Kilobase of exon per Million reads). For real-time PCR, 100 µg of RNA was used for cDNA preparation with an iScript cDNA Synthesis Kit (Bio-Rad, Hercules, CA) according to the manufacturer's protocol. cDNA from each sample was amplified by real-time PCR using iQ SYBR Green Supermix (Bio-Rad). RNA quantities were normalized using GAPDH mRNA as a reference. PCR cycling conditions were as follows: denaturation for 3 min at 95 °C; 40 cycles of amplification for 15 s at 95 °C, 15 s at 60 °C, and 20 s at 70 °C; followed by 30 s at 72 °C. For melting curve analysis, data were collected from 33 cycles (6 s each) with the temperature increased from 60 °C to 92 °C (set point temperature increased after cycle 2 by 1 °C). The primer sets, [*C3*: forward (5′-AGCTTCAGGGTCCCAGC TAC-3′) and reverse (5′-GCTGGAATCTTGATGGAG ACGC-3′), *S100A10*: forward (5′-CCTCTGGCTGTGGA CAAAAT-3′) and reverse (5′-CTGCTCACAAGAAGCAG TGG-3′), g*apdh*: forward (5′-CTCATGACCACAGTCC ATGC-3′ and reverse (5′-TTCAGCTCTGGGATGACCT T-3′)], were used.

Application of the traumatic brain injury (TBI)

All the procedures for the TBI-related animal study were approved by the Institutional Animal Care and Use Committee (IACUC) in the Korea Institute of Science and Technology according to the international standards and guidelines. Wild-type (C57BL/6) mice aged 4 months old were used in this study. The mice were provided with a standard laboratory diet and water ad libitum in a controlled environment. We induced closed diffuse TBI by using a weight-drop device (weight 100 g, fall height 75 cm, angle 90°) as described previously but with a slight modification [22]. The anatomical locus of the impact was adjusted to bregma −1 to ± 4. All the mice were initially anesthetized with an intraperitoneal injection of 2% avertin before receiving the weight-drop–induced TBI. The mice were exposed to a total of 30 impacts (1 in every 3 days for 15 days with a rest of 2 weeks after every 5th impact) using

a single weight (100 g) dropped from a height of 75 cm. Sham-injured animals were subjected to the same protocol of anesthesia, but no weight was used. After TBI, the mice were placed in the supine position in a clean cage heated with a commercially available heating pad. The mice were then returned to their cages after the normal behavior (for example, grooming, walking, and exploring) was recovered.

In situ proximity ligation assay (PLA)

Paraffin-embedded mouse and human brain tissues were sectioned in a coronal plane at 10–20 μm as previously described [23]. The tissue sections were rehydrated, blocked with the blocking solution (1% H_2O_2), and incubated with rabbit anti-calcyon (1:200; Cloud-Clone Corp., PAD980Hu01) and goat anti-hevin (1:200; R&D Systems, AF2728) antibodies overnight at 4 °C. After washing, the sections were incubated with the oligonucleotide-linked secondary antibodies (PLA probes) provided in the kit (Duolink, Sigma-Aldrich Korea, Seoul, South Korea). The oligonucleotides bound to the antibodies were hybridized, ligated, amplified, and detected using a bright-field probe. For nuclear counter staining, the sections were incubated with hematoxylin for 2 min at room temperature. The results were examined by bright-field microscopy.

AMPAR internalization assay

Cortical neurons (DIV10) were treated with several peptides [Hevin (90 nM), ComP2 (25 μg/ml), or ComP2rev (25 μg/ml)] for 1 h and then stimulated with 100 μM AMPA (Sigma-Aldrich) + 1 μM tetrodotoxin (TTX; Tocris Cookson, Inc.) or 1 μM TTX for 15 min at 37°C. Cortical neurons on coverslips were then washed with ice-cold PBS then fixed with 4% paraformaldehyde/ 4% sucrose for 10 min on ice. The coverslips were blocked in 3% BSA / 5% normal donkey serum and incubated with antibodies against the N-terminus of GluA1 (1:50, RH95 clone; Millipore, MAB2263) for 1 h. Cells were washed and incubated with Alexa 488-conjugated secondary antibodies (Jackson ImmunoResearch Laboratories) for 1 h at room temperature. Then, neurons were permeabilized with 0.3% Triton X-100 in PBS for 10 min and incubated with another primary antibody, MAP2 (1:2000, Abcam, ab5392) for 1 h and secondary antibody conjugated to a 594 fluorophore (Jackson ImmunoResearch Laboratories, 111-585-003) for 1 h. After washing with PBS, coverslips were mounted with glass slides for further analysis.

Statistical analysis and data collection

All statistical analyses were performed with GraphPad Prism version 8 (GraphPad Software, Inc., San Diego, CA). Quantitative data were expressed as mean ± standard error of the mean (SEM) of at least three independent experiments. Statistical comparisons were made by a Student's unpaired *t*-test for two groups or one-way analysis of variance (ANOVA) followed by Tukey *post-hoc* test for multiple groups. Sample size of each experimental group/condition was shown in figure legend. No exclusions of data were made that would significantly impact the results or conclusions. The cell lines/animals with the same genotype and similar baseline values were randomly assigned to treated groups. Immunoblotting and reverse transcription PCR data were grouped, but the samples were loaded randomly. The investigator was blinded to the group allocation during the experiment or data acquisition.

Results

Expression of hevin, calcyon, and other synaptic proteins during recovery from brain injury

To explore the astrocytic hevin expression in pathological brain, we monitored the temporal expression pattern of hevin from days 3 to 21 post injury (dpi) in the peri-lesion perimeter using a photothrombotic stroke model (Fig. 1A, B). As previously reported [3], immunohistochemistry data showed that hevin was found in both astrocytes and some neurons in the cortex of the control brain (Fig. 1C and Supplementary Fig. S1A). After brain injury, hevin was predominantly expressed in reactive astrocytes. The number of astrocytes expressing hevin reached a peak at 14-dpi and then significantly decreased at 21-dpi. To determine the relationship between hevin expression and the reactive state of astrocytes in vivo, we used two additional markers of A1- or A2-type reactive astrocytes (C3 or S100A10, respectively) in qPCR and immunohistochemical analysis to further define the reactive state of astrocytes (Supplementary Fig. S2). Our results indicate that C3-positive A1 astrocytes were highly increased at 3- and 5-days postinjury (dpi) but subsequently decreased from 7-dpi. In contrast, S100A10-positive A2 astrocytes were significantly increased at 14-dpi and decreased at 21-dpi. Thus, A1-type astrocytes were dominantly observed during the early phase (3- and 5-dpi), whereas A2-type astrocytes mainly appeared at 14-dpi. In terms of colocalization with hevin, hevin immunoreactivity was negatively correlated with C3-positive A1 astrocytes, as shown in Supplementary Fig. S2 (Pearson correlation = 0.31, hevin+/C3+) and few S100A10-positive A2 astrocytes were found in the peri-injury region at the early phase after brain injury (Supplementary Fig. S2), whereas an increase in hevin-positive astrocytes was observed during this period (Fig. 1C). Thus, hevin expression does not seem to be correlated with either A1 or A2 astrocytes after brain injury.

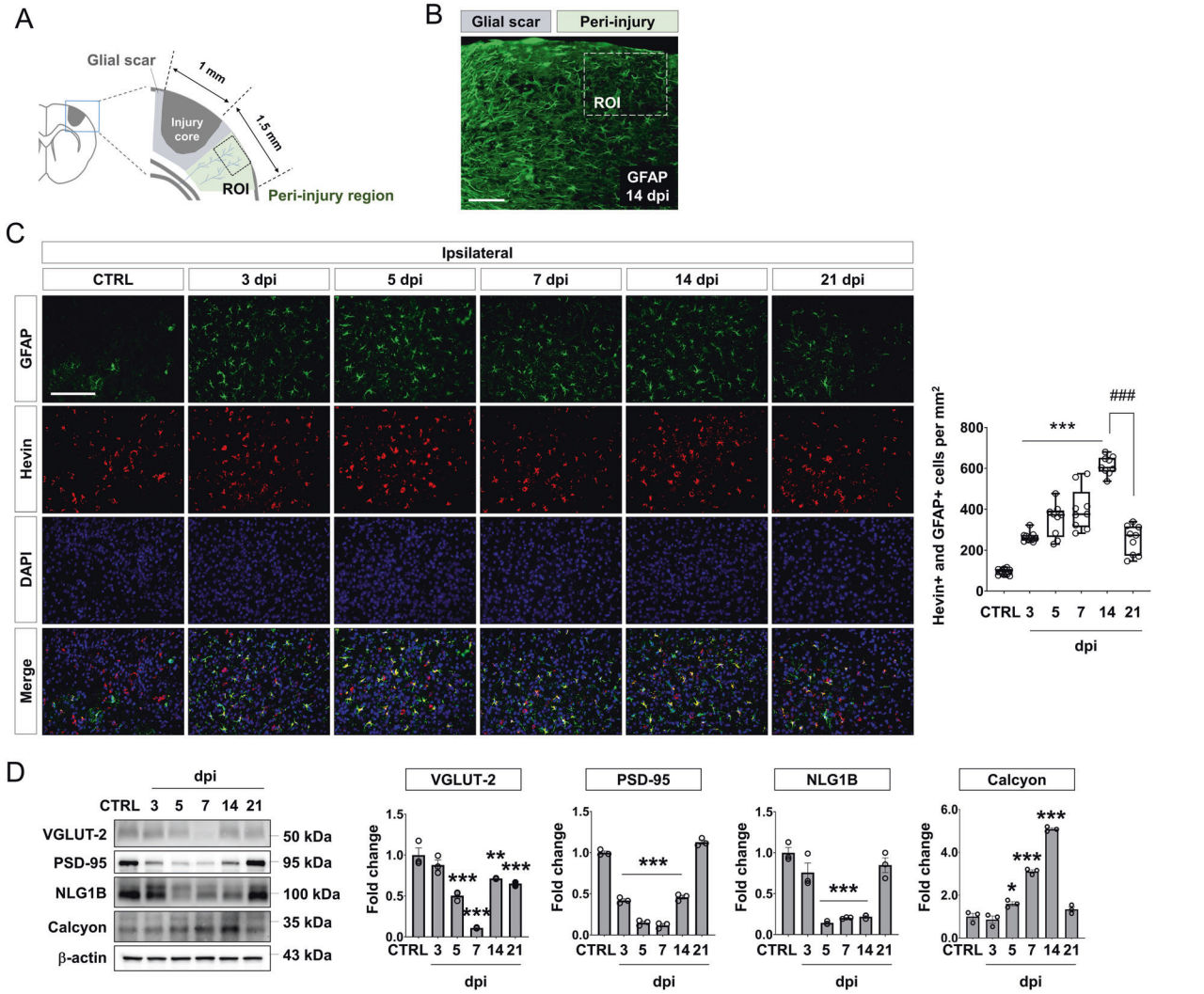

Fig. 1 Spatiotemporal expression of hevin and synaptic proteins following brain injury in the sensory-motor cortical region. A Schematic diagram showing the brain injury region and peri-injury region. Brain injury was generated by photothrombotic stroke. Mice (7–8-week-old) were intraperitoneally injected with Rose Bengal (100 mg per kg, body weight). After 10 min, the sensorimotor cortex was illuminated with a green laser (540 nm, 20 mW) for 20 min. ROI region of interest. **B** Immunohistochemical analysis of GFAP (green) reveals astrogliosis and the peri-injury region at day 14 post-injury (dpi). Scale bar = 100 µm. **C** Colocalization of GFAP (green, 1:1000) and hevin (red, 1:500) in the peri-injury region (scale bar = 200 µm) and quantification of the number of astrocytes (GFAP-positive) expressing hevin (adjacent graph; $n = 9$). DAPI (blue) was used as a counter staining. **D** Immunoblot analysis of synaptic proteins (VGLUT-2, PSD-95, NLG1B, and Calcyon) and quantification of the band intensities (adjacent graphs; $n = 3$). Total protein of 30 µg was loaded onto gels. β-actin was used as a loading control. Data are mean ± SEM. $^{*}p < 0.05$; $^{**}p < 0.01$; $^{***}p < 0.001$ vs. CTRL (control), one-way ANOVA was followed by Tukey *post-hoc* test; $^{\#\#\#}p < 0.001$, 14-dpi. vs. 21-dpi, Student *t*-test.

Next, we assessed the dynamics of synaptic proteins after brain injury (Fig. 1D). Immunoblotting data revealed that the expression of the postsynaptic proteins PSD-95 and NLG1B as well as the presynaptic protein VGLUT-2 gradually decreased and reached the lowest level at 7-dpi. Whereas VGLUT-2 and PSD-95 protein levels recovered at 14-dpi, the level of NLG1B remained low at 14-dpi and returned to the basal level at 21-dpi. Conversely, the expression of the postsynaptic protein calcyon gradually increased and peaked at 14-dpi but decreased at 21-dpi. This protein expression pattern was similar to that of hevin. We asked whether the expression patterns of hevin and calcyon proteins were associated with the recovery from brain injury. For this, we assessed the functional recovery index and astrogliosis (Supplementary Fig. S1B and C). A significant functional recovery was observed from 14-dpi according to the locomotor asymmetry test involving a cylinder (Supplementary Fig. S1B), and the level of the astrogliosis markers (GFAP) and anti-synaptogenic SPARC was highest at 7-dpi but significantly decreased from 14-dpi (Supplementary Fig. S1C) after photothrombotic-stroke–induced sensory-motor cortex injury. These data indicated that the time point

of 14-dpi may be an early recovery phase in our model, and the levels of hevin and calcyon were highest at this time.

Hevin interacts with calcyon

The interaction of hevin with NLG1B has been shown to be crucial in synaptogenesis during CNS development [15]. These synaptogenic proteins may also be involved in synaptic reorganization. However, our data revealed that the NLG1B level remained low at 14-dpi. Therefore, we hypothesized that synaptogenic hevin might interact with calcyon rather than NLG1B at this phase. To test our hypothesis, we employed a yeast two-hybrid assay to assess whether hevin interacted with the extracellular N-terminal region of calcyon (Fig. 2A and Supplementary Fig. S3). Using three kinds of yeast expression vectors carrying the N-terminus of hevin (Hevin-N), C-terminus of hevin (Hevin-C), and N-terminus of calcyon (Calcyon-N), we confirmed that the C-terminus of hevin directly interacted with the N-terminus of calcyon (Fig. 2A). The interaction between calcyon and hevin was also validated by using the biomolecular fluorescence complementation (BiFC) assay (Fig. 2B). In this assay, the N-terminal (VN) and C-terminal halves (VC) of the fluorescent protein Venus fuse, allowing their visualization, only when they are in proximity in the cell. To investigate the intracellular interaction of hevin and calcyon, we generated an expression vector carrying hevin with a VC tag at the C-terminus and without the signal peptide (SP) domain of hevin (Hevin-ΔSP-VC). Then, we compared the hevin-binding capability of N-

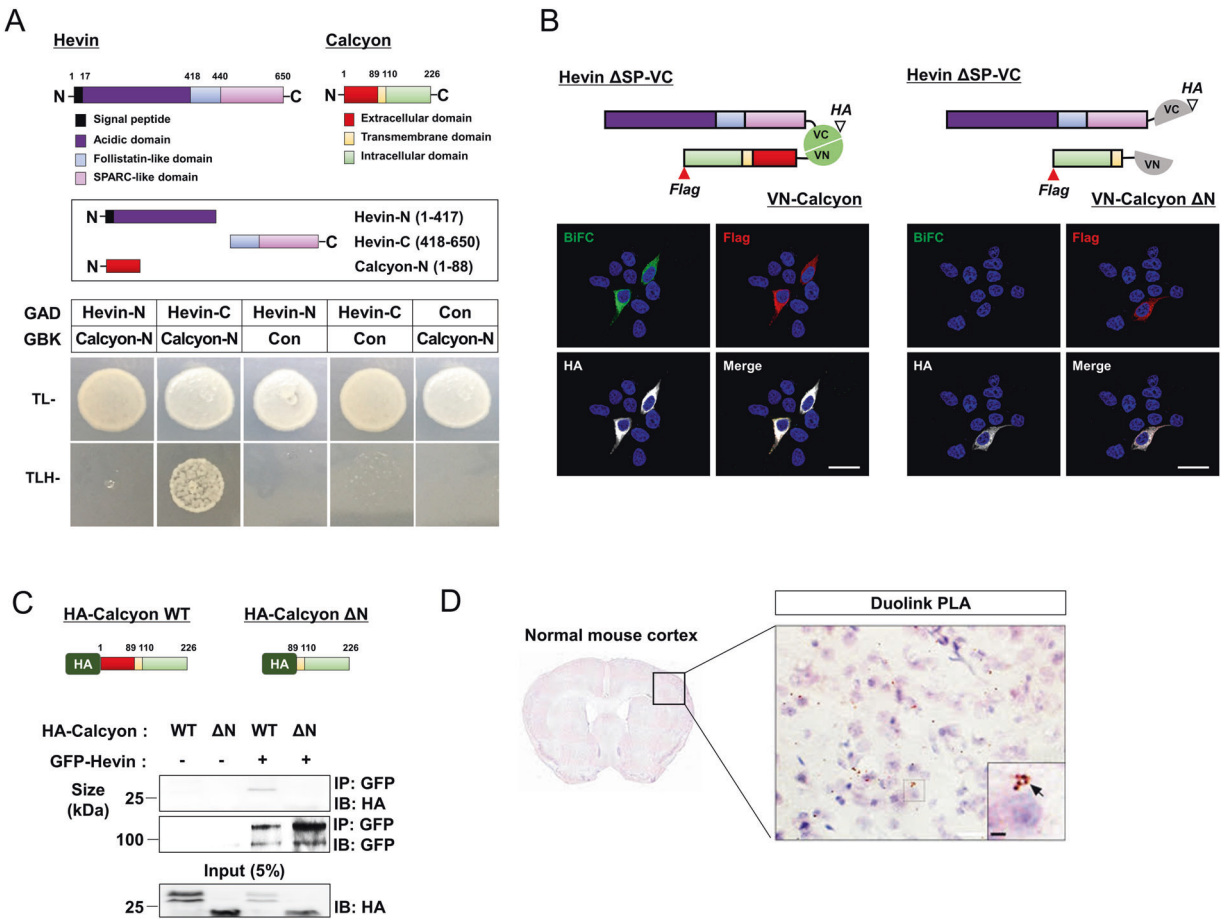

Fig. 2 Hevin interacts with calcyon. A Schematic diagram showing various hevin and calcyon constructs. Calcyon-N was identified as a direct binding partner of Hevin-C using the yeast two-hybrid assay. **B** Bimolecular fluorescence complementation (BiFC) assay. Schematic diagram depicting the BiFC assay. VN and VC are the N-terminal and C-terminal fragments of Venus protein, respectively. Intense Venus signals (green) indicate dimerization (fluorescence complementation). VN-Calcyon strongly interacts with Hevin-ΔSP-VC. Upon deletion of the N-terminus of calcyon (VN-Calcyon ΔN), Venus signals were not detected. Flag (red) and HA (white) staining indicates that transfected vectors were successfully expressed. Nuclei were visualized with DAPI (blue). Scale bar = 25 μm. **C** Coimmunoprecipitation (co-IP) assay. HA-calcyon, HA-calcyon-ΔN, and GFP-Hevin were transfected into HEK293T cells, and cell lysates were then immunoprecipitated using anti-GFP antibody. The immunoprecipitates were examined by immunoblotting using an anti-HA or anti-GFP antibody. Input represents 5% of cell lysates used in the co-IP assay. **D** Representative image of Duolink in situ proximity ligation assay (PLA) in the normal mouse cortex. Arrow indicates the interaction between hevin and calcyon (brown dots).

terminal–truncated calcyon (VN-Calcyon ΔN) with that of full-length calcyon (VN-Calcyon) in HEK293T cells transfected with the two split-BiFC vectors. We confirmed that strong BiFC signals were detected in HEK293T cells transfected with VN-Calcyon and Hevin-ΔSP-VC but not in the cells transfected with VN-Calcyon ΔN and Hevin-ΔSP-VC. Next, to further investigate the interaction between the full-length calcyon and hevin by a mammalian expression system, expression vectors for HA-tagged calcyon (HA-Calcyon WT), calcyon ΔN (HA-Calcyon ΔN), and GFP-tagged hevin (GFP-Hevin) were constructed and expressed in HEK293T cells. We then carried out immunoprecipitation (IP) on cell lysates using an anti-GFP antibody and immunoblotted with an anti-HA antibody. The results showed that GFP-Hevin bound to full-length HA-Calcyon but not to HA-Calcyon ΔN (Fig. 2C). To verify the interaction between endogenous hevin and calcyon in vivo, we conducted a Duolink in situ proximity ligation assay (PLA), which detects the physical proximity between two proteins [24]. PLA data showed an interaction of calcyon and hevin in the cortex of the normal brain (Fig. 2D). Therefore, our results indicated that hevin interacted with calcyon.

The C-terminal region of hevin is essential for its binding to calcyon

To determine the binding domain of hevin that interacts with calcyon, we generated the following three deletion mutant constructs of hevin: (i) hevin 418-E (lacking 1–417), (ii) hevin 436-E (lacking 1–435), and (iii) hevin 540-E (lacking 1–539) (Fig. 3A). Co-IP assay showed that hevin 540-E has a stronger binding affinity than 418-E or 436-E. Next, we generated two C-terminus deletion mutants of hevin 540-E, 540-E Δ40 and 540-E Δ80, and assessed their binding affinities with calcyon. The co-IP assay revealed that calcyon not only interacted with 540-E and 540-E Δ40, but also with the shortest hevin mutant 540-E Δ80 (Fig. 3B). Finally, we found that the 31-amino-acid (540–570) deletion mutant of hevin no longer interacted with calcyon (Fig. 3C), and no BiFC signal was detected (Fig. 3D).

Next, we determined the hevin–calcyon interaction under more physiological condition. For this, we transfected HEK293T cells with several expression vectors containing signal peptide (Hevin-Flag, Hevin-Δ31aa-Flag, and SPARC-Flag) and expression vectors without signal peptide (Hevin-ΔSP-Flag) as a control. Secreted proteins in the conditioned media were concentrated and used for the subsequent experiments (Supplementary Fig. S4). Co-IP experiments were performed using the secreted proteins and lysate of HEK293T cells transfected with Calcyon-HA. As a result, we found that the secreted full-length Hevin, but not 31 aa-deleted form, interacts with calcyon (Fig. 3E), confirming the interaction between hevin and calcyon in the physiological relevant system.

To confirm whether the hevin–calcyon interaction occurs at synapses, we conducted a PLA experiment using a secreted form of hevin protein (hevin-Flag). The primary cultured neurons were transfected with PSD95-mCherry (for the purposes of synapse localization). The transfected neuron cultures were then treated with the secreted form of hevin-Flag. Afterward, antibodies against Flag and extracellular calcyon were used for PLA to determine the hevin–calcyon interaction. As shown in Fig. 3F, secreted soluble hevin also binds to calcyon at the synapses (see the magnified images).

To investigate whether these 31 amino acids were crucial for the interaction between hevin and calcyon, we constructed an mCherry-tagged expression vector for the expression of the fragment encoding for these 31 amino acids and synthesized two split competitive peptides (ComP1 and ComP2) corresponding to these amino acids. Expression of the mCherry-tagged polypeptide composed of the 31 amino acids reduced the binding between hevin and calcyon (Fig. 3G). Moreover, both split competitive peptides also effectively suppressed the interaction of hevin and calcyon. The reversed forms of these peptides ($ComP1_{rev}$ and $ComP2_{rev}$) were used as controls, and they had no inhibitory effect on the interaction (Fig. 3H). These data suggest that the region of hevin between the residues 540–570 is important for interacting with calcyon.

Calcyon and hevin interaction is critical in early synaptic reorganization

To uncover the region-specific role of the interaction between calcyon and hevin in the matured brain, we employed AAV-shRNA-mediated stable knockdown of calcyon (shCalcyon) and hevin (shHevin) (Fig. 4A). In vivo viral infection and knockdown were validated by immunohistochemistry analysis (Supplementary Fig. S5) and immunoblotting (Fig. 4B). First, we assessed synaptic recovery by measuring the synaptic puncta after photothrombotic-stroke–induced sensory-motor cortex injury (Fig. 4C). Brains were isolated at 21-dpi and stained with anti-VGLUT-2 and PSD-95 antibodies. Compared with controls, synaptic reorganization in shCalcyon and shHevin groups were significantly impaired but rescued by co-expression of an shRNA-insensitive form of calcyon ($Calcyon_{ins}$) (Fig. 4C). In addition, we evaluated the functional recovery using the adhesive removal test in shCalcyon and shHevin groups (Fig. 4D and Supplementary Fig. S6). Whereas the tape removal latency of the mice in the control group (scrambled shRNA; Scr) was recovered to that of normal performance (Sham), the mice in shCalcyon and shHevin groups were deficient in tape removal.

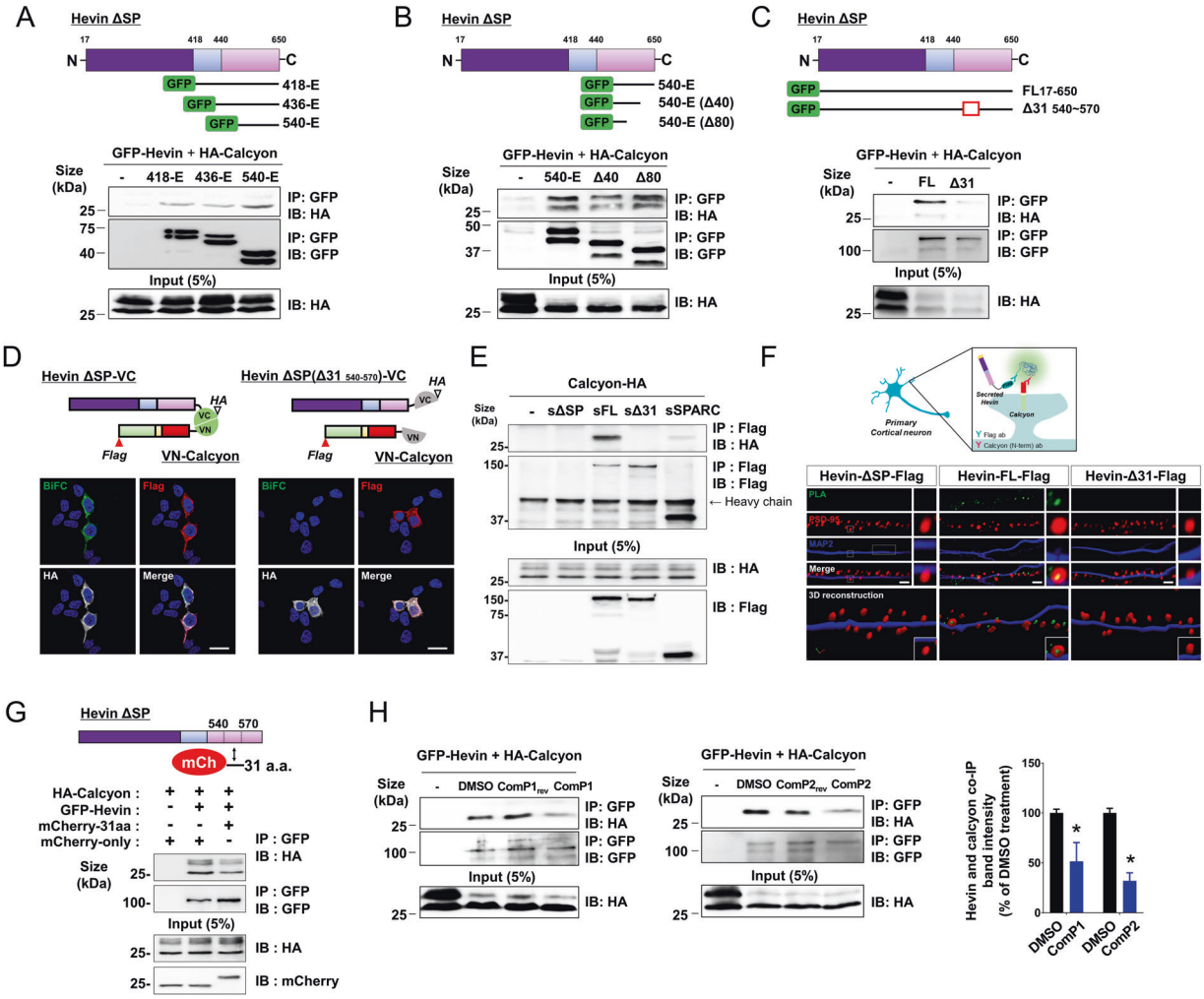

Fig. 3 Identification of an interaction domain between hevin and calcyon. A–C Schematic diagram and co-IP assay to assess for an interaction between HA-tagged mouse calcyon (Calcyon-HA) and the GFP-tagged serial deletion mutants (418-E, 436-E, and 540-E), [540-E, 540-E (Δ40), and 540-E (Δ80)], and full length or mutant [Δ31 (540–570)] hevin. **D** Bimolecular fluorescence complementation (BiFC) assay. Schematic diagram showing the BiFC assay used to assess the interaction between VN-Calcyon and VC-full-length hevin or VC-hevin mutant [Δ31 (540–570)] (*upper*). Intense Venus signals (green) indicate dimerization (*lower*). Hevin lacking the 31 amino acids (aa) [Hevin (Δ31)-VC] no longer interacted with VN-Calcyon. Flag (red) and HA (white) staining indicates that transfected vectors were successfully expressed. Nuclei were visualized with DAPI (blue). Scale bar = 25 μm. **E** Interaction between secreted form of hevin and calcyon. Secreted proteins (Hevin-ΔSP-Flag, Hevin-Flag, Hevin-Δ31aa-Flag, and SPARC-Flag) were mixed with HEK293T cell lysates expressing Calcyon-HA and then immunoprecipitated using anti-Flag antibody. The input represents 5% of mixtures. Secreted SPARC also competed with the secreted form of hevin for calcyon binding. sΔSP, secreted hevin with signal peptide deletion; sFL, secreted form of full-length hevin; sΔ31; secreted hevin with the 31-aa deletion; sSPARC, secreted SPARC. **F** The interaction between hevin and calcyon at the synapses in neurons. Schematic diagram and representative image of the Duolink in situ proximity ligation assay (PLA) assay in the primary cortical neurons (*upper*). Representative images show the PLA signals (green) indicating the interaction between secreted hevin or its deletion mutants and calcyon (*lower*). PSD-95-mCherry (red) was used to visualize post synapses. Scale bar = 5 μm. **G** Competitive inhibition of the interaction between hevin (GFP-Hevin) and calcyon (Calcyon-HA) by mCherry-tagged "31 amino acids" of hevin. Binding affinity was tested using a coimmunoprecipitation assay. **H** Competitive inhibition of the interaction between hevin and calcyon by the synthetic competitive peptides [ComP1 (540–553 a.a.) and ComP2 (554–570 a.a.)] generated from the 31 a.a of hevin. Immunoprecipitation results were quantified by ImageJ software (adjacent graph, $n = 3$). The hevin–calcyon co-IP band intensity was normalized to that obtained under the control condition (DMSO treatment), which was set to 100%. Data are mean ± SEM. $^{*}p < 0.05$ vs. DMSO control, Student *t*-test.

We next tested if the knockdown of either hevin or calcyon affects spontaneous excitatory postsynaptic currents (sEPSCs) during recovery following the cortical injury. At 21-dpi, brain slices were obtained from the virus-infected mice. sEPSCs were recorded from cortical neurons in the damaged cortex (≈ 100 μm). Data revealed that interevent interval (IEI) was significantly increased in shHevin or shCalcyon group compared with scrambled (Scr) shRNA group, but IEI in Calcyon rescue group was reduced to the control level (Scr group) (Fig. 4E).

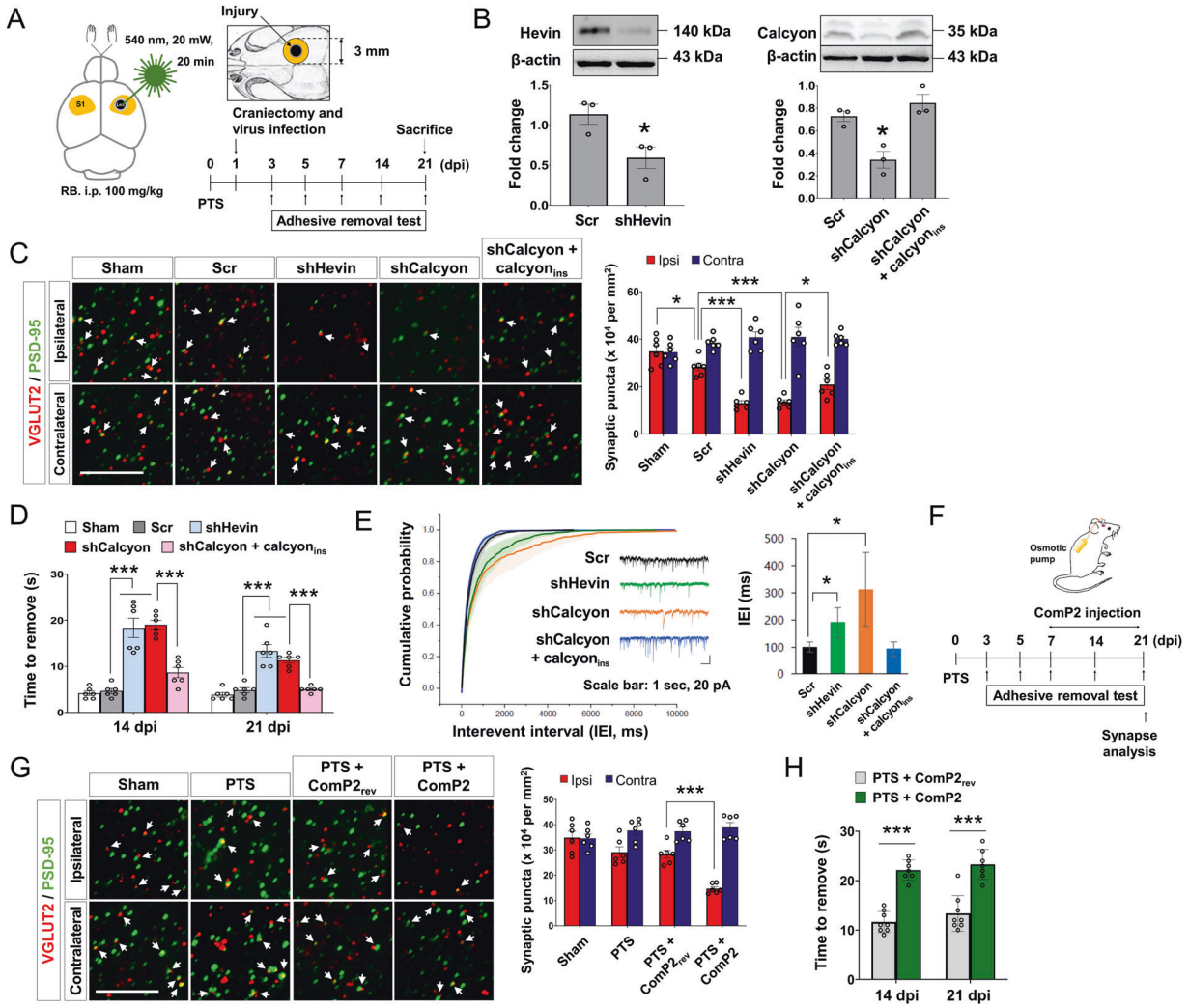

Fig. 4 The role of the hevin–calcyon interaction during synaptic recovery after brain injury. A Schematic presentation of the experimental procedure. Burr hole (3 mm diameter) was generated by craniectomy on the right side of the sensory-motor cortex, and the AAVs were delivered by a gentle drip on the burr hole. PTS photothrombotic stroke, RB Rose Bengal, i.p. intraperitoneal injection. **B** Verification of AAV-mediated knockdown of hevin (shRNA targeting Hevin, shHevin) and calcyon (shRNA targeting Calcyon, shCalcyon) in the peri-injury region after brain injury by using immunoblotting analysis. β-actin was used as a loading control. The rescue of calcyon was performed with co-expression of the shRNA-insensitive form of calcyon ($Calcyon_{ins}$). Adjacent graphs show quantification of band intensity ($n = 3$). $^{*}p < 0.05$ vs. scrambled shRNA (Scr). **C** Synaptogenesis assay in AAV-mediated hevin and calcyon knockdown at 21-dpi. Representative images show synaptic puncta in the peri-injury and contralateral regions. Mice ($n = 6$) were sacrificed at 21-dpi. Brain sections were stained with antibodies against VGLUT2 (red, 1:2000) and PSD-95 (green, 1:500). Arrows indicate colocalization of VGLUT2 and PSD-95-positive puncta. Quantification was performed by semiautomatic counting using the Puncta Analyzer ImageJ plug-in. Scale bar = 5 μm. **D** Adhesive removal test of the AAV-injected mice ($n = 6$ per group). A small adhesive patch (rectangular $0.35 \times 0.45\ cm^2$) was applied to the forelimb contralateral to the photothrombotic hemisphere. The time to make contact and remove the adhesive tape was recorded with 120 s being the time limit. **E** Spontaneous excitatory postsynaptic currents (sEPSCs) during recovery following the cortical injury (21-dpi). Brain slices were obtained from the virus-infected mice. sEPSCs were recorded in cortical neurons from the damaged cortex (≈100 μm). IEI, interevent interval; scale bar = 1 s, 20 pA. **F** Time schedule for hevin competitive peptide 2 (ComP2 or $ComP2_{rev}$, 60 nM) administration using osmotic pump, adhesive removal test, and synapse analysis. **G** Synaptic puncta images and quantification at 21-dpi after the injection of $ComP2_{rev}$ (reverse) and ComP2. Brain sections ($n = 6$) were stained with antibodies against VGLUT2 (red, 1:2000) and PSD-95 (green, 1:500). Arrows indicate colocalization of puncta. Right panel represents quantification of colocalized puncta at 21-dpi. Scale bar = 5 μm. **H** Adhesive removal test of peptide-injected mice ($n = 6$). Data are mean ± SEM. $^{*}p < 0.05$; $^{**}p < 0.01$; $^{***}p < 0.001$, Student *t*-test or one-way ANOVA was followed by Tukey *post-hoc* test.

Amplitude of sEPSC was not significantly different in all groups. These results indicate that hevin, calcyon, and their interaction are critical for reformation of the functional synapse during recovery following brain injury.

In addition, we investigated a functional role of the hevin–calcyon interaction in vivo using binding competitor peptides. We infused the competitive peptide ComP2 using the osmotic pump into the injured region for 2 weeks (from

7-dpi to 21-dpi) after photothrombotic-stroke–induced sensory-motor cortex injury (Fig. 4F). Compared with control (reverse ComP2 peptide; $ComP2_{rev}$), both synaptic puncta organization (Fig. 4G) and behavioral recovery (Fig. 4H) were hindered by infusion of ComP2 peptide. Our data revealed that the genetic and physical inhibition of the interaction between calcyon and hevin caused a significant impairment in synaptic reorganization and functional recovery. This observation suggests that their interaction is pivotal for the early synaptic reorganization.

SPARC interacts with hevin, but is not engaged in synaptic recovery of adult brain

While the expression of hevin continues to increase from the developmental stage to adulthood, the expression of SPARC tends to decrease in the adult brain [3]. We confirmed that SPARC expression was low at 14- and 21-dpi, which corresponds to the synapse recovery period (Supplementary Fig. 1C). Our data indicate that SPARC is able to bind to calcyon and that high expression of SPARC could interfere with the hevin–calcyon interaction (Supplementary Fig. 4D, E). In addition, we found that the affinity of hevin for calcyon was significantly higher than that of SPARC for calcyon (Fig. 3E). Therefore, synaptic recovery in adults is thought to be controlled primarily by hevin rather than by SPARC. To determine the effect of SPARC on synaptic recovery after brain injury, we chronically injected recombinant SPARC protein into the peri-injury region of the cortex from 7-dpi using an osmotic pump. We then compared the synapse number of SPARC-injected mice at 21-dpi with that of vehicle-injected mice (Supplementary Fig. 7). While synapses were restored to almost 80% in the vehicle-injected brain, synaptic recovery was impaired in the SPARC-injected brain. This implies that an injection of SPARC protein at 14-dpi inhibits synaptic recovery.

The synaptogenic activity of hevin is modulated by MMP3 protease in the injured brain

The proteolytic digestion of hevin has previously been documented [17, 25]. Incubation of the full-length hevin with MMP3 or "a disintegrin and metalloproteinase with thrombospondin motifs" (ADAMTS4) protease produced hevin fragments of various sizes. Since both MMP3 and ADAMTS4 are known as inflammatory-regulated proteases [26, 27], we asked whether hevin could be fragmented by MMP3 or ADAMTS4 under pathological conditions. First, we observed that hevin was fragmented in the astrocyte-conditioned media (ACM) derived from an astrocyte culture treated with LPS plus IFN-γ (LPS + IFN) as a neuroinflammatory stimulation (Supplementary Fig. S8A). MMP3 mRNA was highly upregulated in the stimulated astrocytes (Supplementary Fig. S8B). Next, we designed non-contact co-cultures of astrocytes and neurons to further investigate the MMP3-mediated cleavage of hevin (Fig. 5A, B). Astrocytes stimulated with LPS + IFN for 24 h were washed with serum-free media to remove LPS + IFN and other secreted molecules. The washed astrocytes were incubated with recombinant MMP3 protein (rMMP3) or MMP3 inhibitor (MMP3-i) for 24 h, and the ACM was harvested (Fig. 5C). Finally, each ACM was applied to immature cortical neurons at DIV 3, and synapse number was counted at DIV 10 (Fig. 5C). Whereas the synaptic puncta in cortical neurons incubated with the recombinant hevin protein and vehicle-treated control ACM were significantly increased compared with those in normally cultured cortical neurons, the ACM containing rMMP3 and the ACM from astrocytes stimulated with LPS + IFN considerably hindered the synaptogenic effect of the control ACM. In turn, the MMP3 inhibitor attenuated the anti-synaptogenic effect of ACM from astrocytes stimulated with LPS + IFN. These data implied that the hevin could be fragmented by MMP3 to lose the synaptogenic activity under neuroinflammatory conditions.

To extend these analyses to in vivo, we determined whether the persistence of MMP3 level during the early recovery phase could affect synaptic reorganization and functional recovery in the brain. Using a mini-osmotic pump, we infused recombinant MMP3 protein into the sensory-motor cortex injured by a photothrombotic stroke from 7-dpi to 21-dpi. Data showed that the long-term infusion of recombinant MMP3 protein into the injured region significantly reduced the synaptic puncta (Fig. 5D) and behavioral recovery (Fig. 5E). In addition, we explored the temporal pattern of MMP3 and ADAMTS4 mRNA levels after brain injury (Fig. 5F) and found that MMP3 was clearly upregulated from 3-dpi to 7-dpi but diminished from 14-dpi. On the other hand, ADAMTS4 mRNA level was only decreased at 3-dpi and persisted until 21-dpi. While the induction and role of MMP3 are associated with the proinflammatory activity, ADAMTS4 has predominantly an anti-inflammatory effect in the CNS [28]. Therefore, our data suggest that mainly MMP3, rather than ADAMTS4, digests the full-length hevin during acute brain injury. Next, we confirmed whether the MMP3-mediated fragmentation of hevin could affect the interaction between hevin and calcyon. We conducted a co-IP assay using the brain tissue after a photothrombotic stroke (Fig. 5G). The interaction between hevin and calcyon was significantly decreased from 3-dpi to 7-dpi but returned to the basal level at 14-dpi. This interaction pattern was the exact opposite of the MMP3 expression pattern. These observations imply that the elevated MMP3 activity during the acute injury phase cleaves synaptogenic hevin and thereby decreases the interaction between calcyon and hevin.

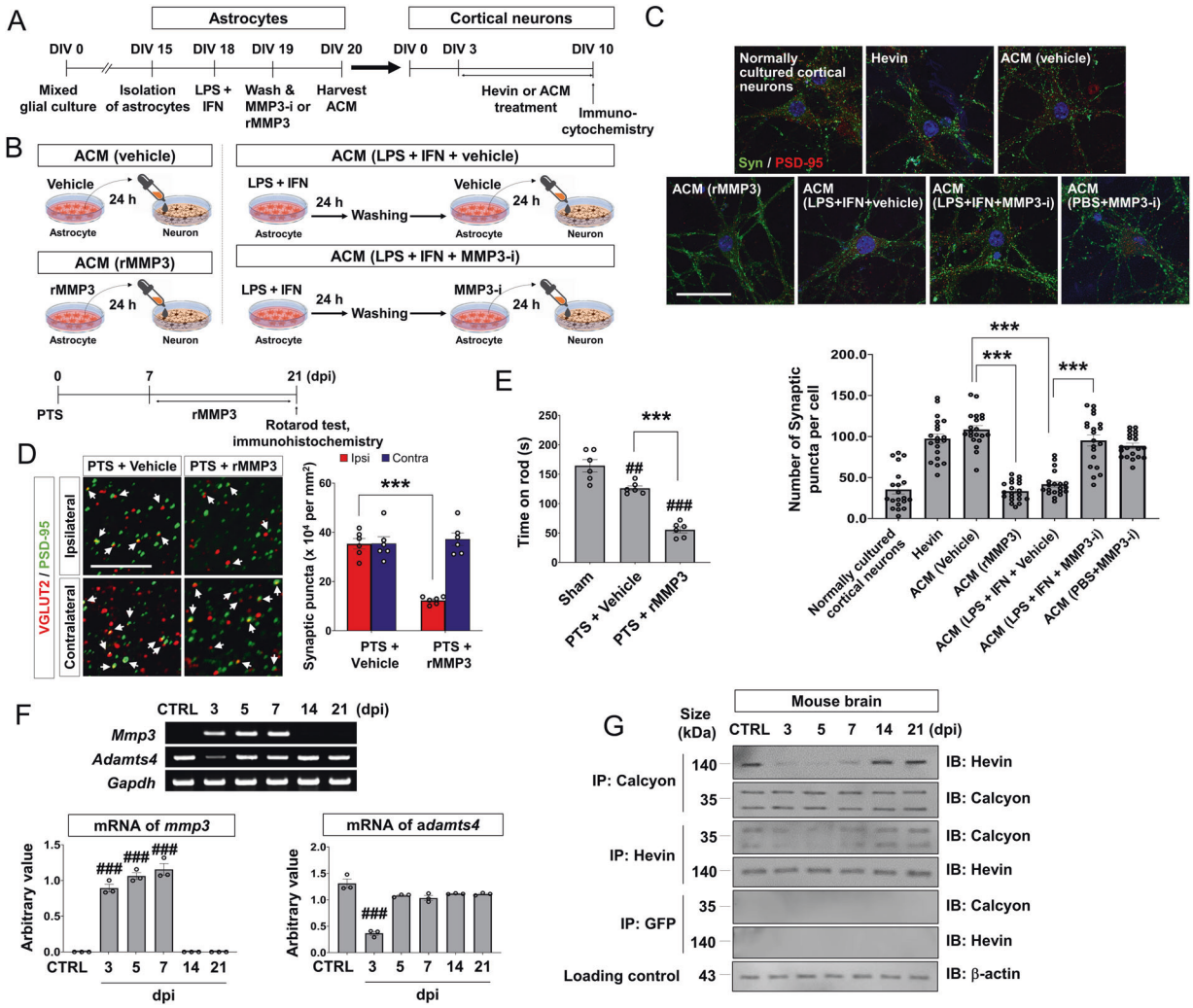

Fig. 5 The synaptogenic function of hevin is modulated by MMP3 under brain injury conditions. A Experimental schedule of in vitro synaptogenesis assay. Astrocytes were isolated from mixed glial cultures at day in vitro (DIV) 15. The astrocytes were incubated with neuroinflammatory stimuli [LPS (1 μg/ml) and IFN-γ (50 units/ml)], MMP3 inhibitor (MMP3-i, 100 μM), or mouse recombinant MMP3 protein (rMMP3, 100 ng) according to the schedule. After treatment, astrocyte-conditioned media (ACM) were administered to cortical neurons with a ratio of 1:1 (ACM: neuron culture media) and immunocytochemical analysis (ICC) was performed. **B** Schematic drawing of ACM acquisition and administration to cortical neurons. **C** Synaptogenesis assay on ACM-treated cortical neurons. Cells (n = 20) were stained with antibodies against Synaptotagmin (Syn, green, 1:1000) and PSD-95 (red, 1:500). Images were obtained by confocal microscopy (*upper*). Synapse number was quantified using the ImageJ plug-in with the colocalized fluorescence signals of presynaptic synaptotagmin (Syn) and PSD-95 (*lower*). Normally cultured cortical neurons were used as a control. ACM and mouse recombinant hevin protein (60 nM) were used as a synaptogenic control. Scale bar = 20 μm. **D** Effect of MMP3 infusion on the synaptic reorganization. Mice (n = 6) were sacrificed at 21-dpi. Brain sections were stained with antibodies against VGLUT2 (red, 1:2000) and PSD-95 (green, 1:500). Arrows indicate colocalization of puncta. Right panel represents quantification of colocalized puncta. Synaptic puncta were analyzed by using ImageJ plugin. Scale bar = 5 μm. **E** The functional recovery of mice treated with MMP3 protein was assessed by the Rotarod test. Mice ($n = 6$) were tested in 3 trials for 5 min each (4–40 rpm). **F** Time course of *mmp3* and *adamts4* mRNA expression after brain injury. The expression was evaluated by conventional RT-PCR (*upper*) and quantification (*lower*). Band intensities of *mmp3* and *adamts4* were normalized to that of *gapdh* ($n = 3$). **G** Representative gel images of control or PTS mouse brain tissue subjected to co-IP between hevin and calcyon. Data are mean ± SEM. $^{***}p < 0.001$, Student *t*-test. $^{\#\#}p < 0.01$; $^{\#\#\#}p < 0.001$, one-way ANOVA was followed by Tukey *post-hoc* test.

Hevin increases surface expression of AMPAR and promotes functional synapse formation

A recent report demonstrated that hevin promotes formation of functional synapses in cultured cortical neurons [29], in contrast to previous findings in purified retinal ganglion cells (RGCs) [3]. Interestingly, in our study, we showed that treatment of cortical neurons with hevin not only increased the number of synapses (Fig. 5C), but also the amount of AMPAR on the cell surface

(Supplementary Fig. S9A–C). In addition, we found that both amplitude and frequency were increased by hevin treatment in AMPA-mediated EPSC under the same conditions (Supplementary Fig. S9D). Although the electrophysiology data obtained from brain slices showed changes in EPSC frequency but not amplitude during injury recovery (Fig. 4E), this result may have been due to spontaneous postsynaptic currents (PSCs) containing both glutamatergic and GABAergic synaptic currents. Therefore, we speculate that, unlike in cultured conditions, the lack of difference in amplitude observed from brain slice analysis might have emerged from the synaptic contamination during GABAergic synapse formation at the recovery phase. For clarification, additional experiments might be required to investigate mEPSCs or mIPSCs from the same conditions of slice recording. Nevertheless, we believe that our results (i.e., AMPAR staining and electrophysiological data) from analysis of cultured neurons support our hypothesis that hevin contributes to the formation of functional synapses in the brain.

Hevin promotes both VGLUT1+ and 2+ synaptogenesis in the cortex

Previously, hevin has been shown to specifically induce VGLUT2+ thalamocortical synapses but not to induce VGLUT1+ synapses in cortical neuron-only cultures [7]. However, our data showed that hevin induces excitatory synapses (syn/PSD95) in cortical neurons (Fig. 5C). Therefore, we reevaluated the effect of hevin on the VGLUT1+ or 2+ synaptogenesis under conditions in which cortical neurons were cultivated alone or cocultured with thalamic neurons mixed with a small number of astrocytes (Supplementary Fig. S10). Having analyzed 40 cells in each condition, we found that VGLUT2+ synapses were increased following hevin treatment in cultured cortical neurons alone as well as in the coculture condition. In addition, the VGLUT1+ synapse was also significantly increased after hevin treatment under both culture conditions, which is consistent with the recently published results of Gan et al. [30]. Therefore, although hevin is known to primarily induce the VGLUT2+ thalamocortical synapse, it may also be involved in the generation of both VGLUT1+ and VGLUT2+ synapses in the cortex.

Interaction of calcyon and hevin in the mouse and human brain after traumatic brain injury

To test whether the regulation of synaptogenic hevin function by MMP3 can be considered a general observation under pathological conditions, we examined the hevin expression and the interaction between calcyon and hevin in a traumatic brain injury (TBI) model. We employed the weight-drop TBI model, which mimics a repetitive brain injury in humans and provides the following merits: (i) it is simple and easy to apply consistent repetitive hits and (ii) it represents the pathophysiological features and symptoms of concussion [22]. Similarly to the photothrombotic stroke model (Fig. 1), hevin was upregulated in the reactive astrocytes (Fig. 6A), and the PLA data revealed that the interaction between hevin and calcyon was significantly decreased in the TBI model (Fig. 6B). Consistently, PLA signals were observed in the gray matter but not in the white matter of the frontal cortex of the normal human brain but rarely detected in the postmortem brain with chronic traumatic encephalopathy (CTE) (Fig. 6C). In addition, we confirmed whether our previous observations of hevin fragmentation and MMP3 expression in the animal model were also found in the brain of CTE patients. The immunoblotting data revealed that the total protein levels of hevin and calcyon were not significantly different but hevin fragmentation was increased in the CTE brain (Fig. 6D). Concurrently, the MMP3 mRNA levels in the CTE brain were considerably increased (Fig. 6E).

Discussion

In the present study, we evaluated the spatiotemporal dynamics of hevin expression after brain injury. We demonstrated, for the first time, a proteolytic modulation of hevin under brain injury condition, rather than brain development. Since MMP3, an inducible protease during acute injury phase, generates a hevin fragment of an apparent molecular size similar to that of intact SPARC [17], the proteolytic modulation of hevin may be a neuroprotective event at the acute phase after a brain insult [3, 31, 32].

We found that the extracellular domain of calcyon strongly interacted with the C-terminus of hevin (Figs. 2 and 3), and this interaction might be required in the early synaptic recovery (Fig. 4). Previously, hevin has been shown to connect neurexin-1α and NLG1 to assemble glutamate synapses [15]. However, our findings suggest a different molecular mechanism of synapse modulation following brain injury. The synaptogenic activity of hevin for an early synaptic reorganization may be fulfilled by interacting with calcyon rather than NLG1 or neurexin-1α.

Our study suggested a novel role of the extracellular domain of calcyon as a synaptic cell adhesion molecule facilitating synaptic contacts. We showed that hevin hampered the calcyon-mediated internalization of AMPA receptor in neuronal cells via molecular interaction between hevin and the extracellular domain of calcyon (Supplementary Fig. S11), although the detailed mechanism remains elusive and should be deciphered in a further study. Thus, it is likely that, during early synaptic recovery phase, calcyon may play a more important role in the synaptic

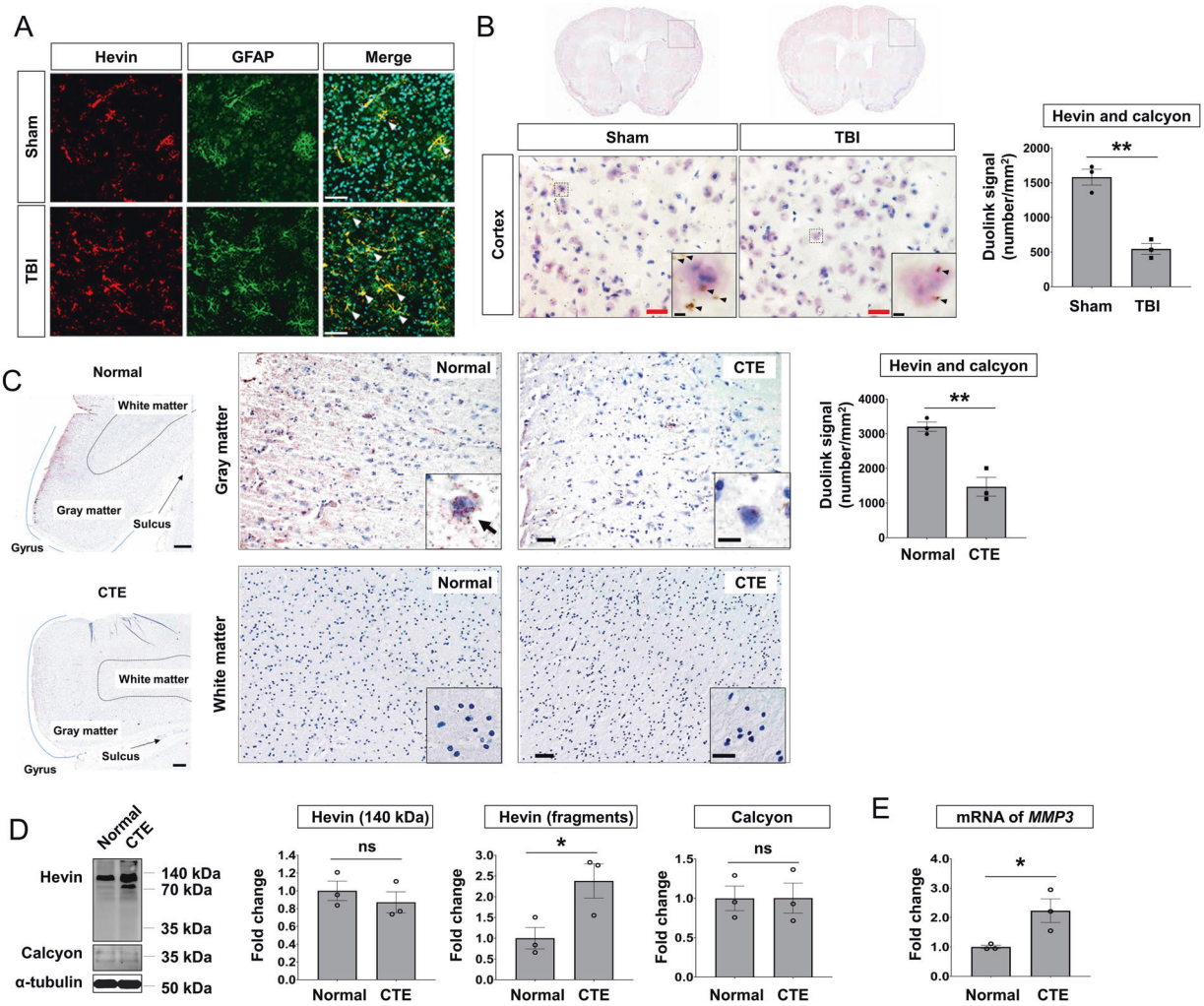

Fig. 6 Interaction between hevin and calcyon in the pathological brain of traumatic brain injury (TBI) model and chronic traumatic encephalopathy patients. **A** Colocalization of hevin with GFAP in the sham and TBI mouse brain. The fluorescence intensity of hevin was increased in GFAP-positive cells (marked with white arrowheads) of TBI mouse model. Scale bar = 50 μm. **B** Duolink in situ proximity ligation assay (PLA) detection of interaction between hevin and calcyon in the sham and TBI mouse brain. Signals appear as brown dots and are marked with the black arrowheads. Scale bars = 20 μm (red) and 5 μm (black). Quantification of Duolink signal is shown in the right panel ($n = 3$). **C** Duolink in situ PLA detection of the interaction between hevin and calcyon in the cortical region of Chronic Traumatic Encephalopathy (CTE) patient brain. Signals appear as brown dots and are marked with arrow. Scale bar represents 1 mm (in the left panel), 50 μm (large square in the middle panel), and 5 μm (small square in the middle panel). Quantification of Duolink signals is shown in the right panel ($n = 3$). **D** Immunoblot of hevin and calcyon using postmortem brain tissue of normal and CTE patients. Quantification of immunoblot analysis is shown in the adjacent graphs ($n = 3$). Hevin fragmentation was represented as the intensity of fragment per total hevin. α-tubulin was used as a loading control. **E** Alteration of *MMP3* mRNA expression in the normal and CTE patient brain ($n = 3$ per group) based on RNA-seq data. Data are mean ± SEM. $^{*}p < 0.05$; $^{**}p < 0.01$, Student *t*-test. ns not significant.

adhesion by interacting with hevin, rather than its regulatory role in a synaptic activity [33–36].

Taken together, our investigation demonstrates the novel interaction between calcyon and hevin as well as the role of the interaction under pathological brain conditions. We found a critical event associated with synaptogenic hevin and a novel function of calcyon acting as a synaptic accessory protein, based on spatiotemporal regulation during early synaptic recovery following brain injury. Over the past decade, it has been shown that numerous individuals who survive post-brain injury suffer from severe and permanent neurological dysfunctions [37], such as cognitive deficits [30] or epileptic seizures [38]. These conditions may be due to abnormal synaptic organization. Accordingly, it has been suggested that a correlation between synaptic abnormality and neuroinflammation is closely associated with cognitive vulnerability [39]. Glia cells are believed to play a crucial role in the synaptic organization as well as neuronal connectivity. Therefore, understanding the temporal dynamics of astrocyte activation and astrocyte-derived matricellular proteins during synaptic organization will contribute to finding novel therapeutic strategies for neurological dysfunctions associated with brain injury.

Author contributions JHK, EMH, and KS designed the research. JHK and JH conducted animal experiments and acquired the data. HGJ, AK, SJH, YSL, and EMH provided the AAV-shRNA and conducted the Co-IP assay. JHJ and JKL carried out electrophysiological experiments. HSS and HR performed immunohistochemistry and real-time PCR on human brain tissues. JHK, HGJ, and AK analyzed the data. JHK, EMH, and KS drafted the manuscript, with final editing by all the authors. EMH and KS supervised the work.

Funding This work was supported by a grant from the Basic Science Research Program through the National Research Foundation (NRF), which is funded by the Korean government (Ministry of Science, ICT and Future Planning, MSIP) (2016M3C7A1904148, 2017M3C7A1043842, and NRF-2020M3E5D9079764).

Compliance with ethical standards

Conflict of interest The authors declare no competing interests.

Ethical approval The current study was approved by the appropriate local ethics committee. Neuropathological processing of control and CTE human brain samples was performed according to the procedures previously established by the BUADC and CTE Center. Institutional review board approval for ethical permission was obtained through the BUADC and CTE Center [40, 41]. This study was reviewed by the Boston University School of Medicine Institutional Review Board (Protocol H-28974) and was approved as exempt because the study involved only tissue collected from post-mortem individuals that are not classified as human subjects. Nevertheless, next of kin provided informed consent for participation and brain donation. The study was performed in accordance with the institutional regulatory guidelines and principles of human subject protection in the Declaration of Helsinki. All animal care and handling were approved by the institutional guidelines of Institutional Animal Care and Use Committee at the Korea Institute of Science and Technology (IACUC-2017-056) and Kyungpook National University Animal Care Committee (KNU 2019-90).

Publisher's note Springer Nature remains neutral with regard to jurisdictional claims in published maps and institutional affiliations.

References

1. Araque A, Parpura V, Sanzgiri RP, Haydon PG. Tripartite synapses: glia, the unacknowledged partner. Trends Neurosci. 1999;22:208–15.
2. Chung WS, Allen NJ, Eroglu C. Astrocytes control synapse formation, function, and elimination. Cold Spring Harb Perspect Biol. 2015;7:a020370.
3. Kucukdereli H, Allen NJ, Lee AT, Feng A, Ozlu MI, Conatser LM, et al. Control of excitatory CNS synaptogenesis by astrocyte-secreted proteins Hevin and SPARC. Proc Natl Acad Sci USA. 2011;108:E440–449.
4. Christopherson KS, Ullian EM, Stokes CC, Mullowney CE, Hell JW, Agah A, et al. Thrombospondins are astrocyte-secreted proteins that promote CNS synaptogenesis. Cell. 2005;120:421–33.
5. Jones EV, Bouvier DS. Astrocyte-secreted matricellular proteins in CNS remodelling during development and disease. Neural Plast. 2014;2014:321209.
6. Risher WC, Patel S, Kim IH, Uezu A, Bhagat S, Wilton DK, et al. Astrocytes refine cortical connectivity at dendritic spines. eLife. 2014;3:e04047.
7. Burda JE, Sofroniew MV. Reactive gliosis and the multicellular response to CNS damage and disease. Neuron. 2014;81:229–48.
8. Clarke LE, Barres BA. Emerging roles of astrocytes in neural circuit development. Nat Rev Neurosci. 2013;14:311–21.
9. Liauw J, Hoang S, Choi M, Eroglu C, Choi M, Sun GH, et al. Thrombospondins 1 and 2 are necessary for synaptic plasticity and functional recovery after stroke. J Cereb Blood Flow Metab. 2008;28:1722–32.
10. Schwab JM, Beschorner R, Nguyen TD, Meyermann R, Schluesener HJ. Differential cellular accumulation of connective tissue growth factor defines a subset of reactive astrocytes, invading fibroblasts, and endothelial cells following central nervous system injury in rats and humans. J Neurotrauma. 2001;18:377–88.
11. Ikeshima-Kataoka H, Shen JS, Eto Y, Saito S, Yuasa S. Alteration of inflammatory cytokine production in the injured central nervous system of tenascin-deficient mice. Vivo. 2008;22:409–13.
12. Adams JC. Functions of the conserved thrombospondin carboxy-terminal cassette in cell-extracellular matrix interactions and signaling. Int J Biochem Cell Biol. 2004;36:1102–14.
13. Nishio T, Kawaguchi S, Iseda T, Kawasaki T, Hase T. Secretion of tenascin-C by cultured astrocytes: regulation of cell proliferation and process elongation. Brain Res. 2003;990:129–40.
14. Strekalova T, Sun M, Sibbe M, Evers M, Dityatev A, Gass P, et al. Fibronectin domains of extracellular matrix molecule tenascin-C modulate hippocampal learning and synaptic plasticity. Mol Cell Neurosci. 2002;21:173–87.
15. Singh SK, Stogsdill JA, Pulimood NS, Dingsdale H, Kim YH, Pilaz LJ, et al. Astrocytes assemble thalamocortical synapses by bridging NRX1alpha and NL1 via Hevin. Cell. 2016;164:183–96.
16. Yang Y, Rosenberg GA. Matrix metalloproteinases as therapeutic targets for stroke. Brain Res. 2015;1623:30–38.
17. Weaver M, Workman G, Schultz CR, Lemke N, Rempel SA, Sage EH. Proteolysis of the matricellular protein hevin by matrix metalloproteinase-3 produces a SPARC-like fragment (SLF) associated with neovasculature in a murine glioma model. J Cell Biochem. 2011;112:3093–102.
18. Ippolito DM, Eroglu C. Quantifying synapses: an immunocytochemistry-based assay to quantify synapse number. J Vis Exp. 2010;45:2270.
19. McCarthy KD, de Vellis J. Preparation of separate astroglial and oligodendroglial cell cultures from rat cerebral tissue. J Cell Biol. 1980;85:890–902.
20. Jo M, Kim JH, Song GJ, Seo M, Hwang EM, Suk K. Astrocytic orosomucoid-2 modulates microglial activation and neuroinflammation. J Neurosci. 2017;37:2878–94.
21. Chevallet M, Diemer H, Van Dorssealer A, Villiers C, Rabilloud T. Toward a better analysis of secreted proteins: the example of the myeloid cells secretome. Proteomics. 2007;7:1757–70.
22. Seo JS, Lee S, Shin JY, Hwang YJ, Cho H, Yoo SK, et al. Transcriptome analyses of chronic traumatic encephalopathy show alterations in protein phosphatase expression associated with tauopathy. Exp Mol Med. 2017;49:e333.
23. Lee J, Kim Y, Liu T, Hwang YJ, Hyeon SJ, Im H, et al. SIRT3 deregulation is linked to mitochondrial dysfunction in Alzheimer's disease. Aging Cell. 2018;17:e12679.
24. Soderberg O, Gullberg M, Jarvius M, Ridderstrale K, Leuchowius KJ, Jarvius J, et al. Direct observation of individual endogenous protein complexes in situ by proximity ligation. Nat Methods. 2006;3:995–1000.
25. Weaver MS, Workman G, Cardo-Vila M, Arap W, Pasqualini R, Sage EH. Processing of the matricellular protein hevin in mouse brain is dependent on ADAMTS4. J Biol Chem. 2010;285:5868–77.
26. Lemarchant S, Pruvost M, Montaner J, Emery E, Vivien D, Kanninen K, et al. ADAMTS proteoglycanases in the

physiological and pathological central nervous system. J Neuroinflammation. 2013;10:133.
27. Cunningham LA, Wetzel M, Rosenberg GA. Multiple roles for MMPs and TIMPs in cerebral ischemia. Glia. 2005;50:329–39.
28. Gottschall PE, Howell MD. ADAMTS expression and function in central nervous system injury and disorders. Matrix Biol. 2015;44-46:70–76.
29. Gan KJ, Sudhof TC. SPARCL1 promotes excitatory but not inhibitory synapse formation and function independent of neurexins and neuroligins. J Neurosci. 2020;40:8088–102.
30. de Freitas Cardoso MG, Faleiro RM, de Paula JJ, Kummer A, Caramelli P, Teixeira AL, et al. Cognitive impairment following acute mild traumatic brain injury. Front Neurol. 2019; 10:198.
31. Li T, Tan X, Zhu S, Zhong W, Huang B, Sun J, et al. SPARC induces phenotypic modulation of human brain vascular smooth muscle cells via AMPK/mTOR-mediated autophagy. Neurosci Lett. 2019;712:134485.
32. Lloyd-Burton SM, York EM, Anwar MA, Vincent AJ, Roskams AJ. SPARC regulates microgliosis and functional recovery following cortical ischemia. J Neurosci. 2013;33:4468–81.
33. Yin DM, Chen YJ, Liu S, Jiao H, Shen C, Sathyamurthy A, et al. Calcyon stimulates neuregulin 1 maturation and signaling. Mol Psychiatry. 2015;20:1251–60.
34. Ha CM, Park D, Han JK, Jang JI, Park JY, Hwang EM, et al. Calcyon forms a novel ternary complex with dopamine D1 receptor through PSD-95 protein and plays a role in dopamine receptor internalization. J Biol Chem. 2012;287:31813–22.
35. Davidson HT, Xiao J, Dai R, Bergson C. Calcyon is necessary for activity-dependent AMPA receptor internalization and LTD in CA1 neurons of hippocampus. Eur J Neurosci. 2009;29:42–54.
36. Xiao J, Dai R, Negyessy L, Bergson C. Calcyon, a novel partner of clathrin light chain, stimulates clathrin-mediated endocytosis. J Biol Chem. 2006;281:15182–93.
37. Rosenfeld JV, Maas AI, Bragge P, Morganti-Kossmann MC, Manley GT, Gruen RL. Early management of severe traumatic brain injury. Lancet. 2012;380:1088–98.
38. Perucca P, Smith G, Santana-Gomez C, Bragin A, Staba R. Electrophysiological biomarkers of epileptogenicity after traumatic brain injury. Neurobiol Dis. 2019;123:69–74.
39. Delpech JC, Madore C, Nadjar A, Joffre C, Wohleb ES, Laye S. Microglia in neuronal plasticity: Influence of stress. Neuropharmacology. 2015;96:19–28. (Pt A)
40. Mez J, Solomon TM, Daneshvar DH, Murphy L, Kiernan PT, Montenigro PH, et al. Assessing clinicopathological correlation in chronic traumatic encephalopathy: rationale and methods for the UNITE study. Alzheimers Res Ther. 2015;7:62.
41. Vonsattel JP, Amaya Mdel P, Cortes EP, Mancevska K, Keller CE. Twenty-first century brain banking: practical prerequisites and lessons from the past: the experience of New York Brain Bank, Taub Institute, Columbia University. Cell Tissue Bank. 2008;9:247–58.